



Article

Low-Threshold, Multiple High-Order Harmonics Fiber Laser Employing $\text{Cr}_2\text{Si}_2\text{Te}_6$ Saturable Absorber

Nannan Xu ^{1,2}, Xinxin Shang ^{1,2} , Shuo Sun ³ , Fuhao Yang ³, Weiyu Fan ³, Huanian Zhang ^{3,*} and Dengwang Li ^{1,2,*}

¹ Shandong Province Key Laboratory of Medical Physics and Image Processing Technology, School of Physics and Electronics, Shandong Normal University, Jinan 250014, China

² Shandong Provincial Key Laboratory of Optics and Photonic Device, School of Physics and Electronics, Shandong Normal University, Jinan 250014, China

³ School of Physics and Optoelectronic Engineering, Shandong University of Technology, Zibo 255049, China

* Correspondence: huanian_zhang@163.com (H.Z.); dengwang@sdnu.edu.cn (D.L.)

Abstract: Abundant research findings have proved the value of two-dimensional (2D) materials in the study of nonlinear optics in fiber lasers. However, there remains two problems: how to reduce the start-up threshold, and how to improve the damage threshold, of fiber lasers based on 2D materials. A 15.1 mW low-threshold mode-locked fiber laser, based on a $\text{Cr}_2\text{Si}_2\text{Te}_6$ saturable absorber (SA) prepared by the liquid-phase exfoliation method, is demonstrated successfully in this work. This provides a useful and economical method to produce SAs with low insertion loss and low saturation intensity. Besides, multiple high-order harmonics, from the fundamental frequency (12.6 MHz) to the 49th-order harmonic (617.6 MHz), mode-locked operations are recorded. The experimental results indicate the excellent potential of $\text{Cr}_2\text{Si}_2\text{Te}_6$ as an optical modulator in exploring the soliton dynamics, harmonic mode locking, and other nonlinear effects in fiber lasers.

Keywords: low-threshold fiber laser; harmonic mode locking; 2D material



Citation: Xu, N.; Shang, X.; Sun, S.; Yang, F.; Fan, W.; Zhang, H.; Li, D. Low-Threshold, Multiple High-Order Harmonics Fiber Laser Employing $\text{Cr}_2\text{Si}_2\text{Te}_6$ Saturable Absorber. *Nanomaterials* **2023**, *13*, 1038. <https://doi.org/10.3390/nano13061038>

Academic Editors: Alexander Tselev and Béla Pécz

Received: 28 January 2023

Revised: 12 February 2023

Accepted: 8 March 2023

Published: 14 March 2023



Copyright: © 2023 by the authors. Licensee MDPI, Basel, Switzerland. This article is an open access article distributed under the terms and conditions of the Creative Commons Attribution (CC BY) license (<https://creativecommons.org/licenses/by/4.0/>).

1. Introduction

Two-dimensional (2D) materials, with a van der Waals layered structure, possess attractive properties including quantum effects, microsize effects, and surface effects, for technical and practical applications such as in biomedicine, optical sensors, photodetectors, ultrafast photonics, and optical modulations [1–8]. Especially, distinctive physical singularities will occur as charge or heat transfer are determined on a plane, which has aroused the interest of researchers. One of the most active research directions is the preparation of 2D materials-based saturable absorbers (SAs) and their corresponding application in ultrafast fiber lasers [9–12]. This has great significance for the exploration of soliton dynamics, harmonic mode locking, and abundant other and complex nonlinear optical effects. The nonlinear saturable absorption effect is the basis of 2D materials used as SAs. The mechanism of saturation absorption of an SA is the Pauli blocking principle. When high-intensity light enters, the electrons in the 2D material will be excited from the valence band to the conduction band. After the conduction band is completely occupied, the photons will no longer be absorbed by the material, and SAs will show the saturable absorption property. Since the ultrafast fiber lasers realized by SAs have the advantages of simple structure and low cost [13], researchers have never stopped looking for more improved 2D materials, with better nonlinear effects and exceptional air stability, to realize excellent laser output.

There are two problems: (i) how to reduce the start-up threshold, and (ii) how to improve the damage threshold of fiber lasers based on 2D materials, that researchers are attempting to solve [9,14]. Among them, low-threshold fiber lasers have attracted great attention due to their advantages: a low mode-locked threshold means that ultrashort pulses can be obtained under a low operating voltage and current, corresponding to a low

cost. Besides, a lower threshold leads to a lower intensity of spontaneous radiation noise and so the laser can operate with better stability. In addition, in the field of biomedicine, low-power lasers are needed, since proteins are vulnerable to damage in strong light fields. So low-threshold ultrafast lasers have great application potential. Currently, research on fiber lasers with a low threshold is developing rapidly [15–17]. The threshold concept arises due to the inevitable presence of self-radiating noise in fiber lasers [18], the magnitude of which can be reduced, but not eliminated completely. The advantages of low-threshold fiber lasers are also indirectly demonstrated by the direct relationship between the laser generation threshold and the laser emission. Therefore, it is important to study the factors affecting the start-up threshold, and to provide solutions. We find that, in addition to the self-radiating noise of fiber lasers, there are some crucial factors that affect the start-up threshold of 2D materials-based fiber lasers, which are, insertion loss and saturation intensity of 2D materials-based SAs. So, finding a suitable material, and optimizing the preparation method of SAs, is one of the ideas to reduce the start-up threshold.

Due to the continuous exploration in the field of materials, various materials have been applied to the research of low-threshold mode-locked fiber lasers, since graphene [19–24]. The availability of topological insulators (TIs) offers the possibility of making high-performance SAs [25–27]. Yin et al. prepared a Bi_2Te_3 -based SA and output mode-locked pulses, with a pulse width of 1.26 ps, but the threshold power was still as high as 315 mW [28]. The appearance of black phosphorus (BP) provided researchers with more options to improve the performance of mode-locked fiber lasers [29,30]. Yu et al. prepared a BP-based SA, with a modulation depth of ~9.8%, and a mode-locked laser output with a pulse width of 1.58 ps was achieved, at a threshold power of 303 mW [31]. Later, transition metal dichalcogenides (TMDs) were extensively studied [32,33]. Lee et al. prepared a molybdenum diselenide (MoSe_2) SA, by a liquid-phase exfoliation (LPE) method, and it was successfully applied in a fiber laser, with a threshold power of 274 mW [34]. Wu et al. achieved mode-locked operation in a fiber laser by using tungsten disulfide (WS_2), at 1500 nm, for which the pump power reached 260 mW [35]. Some newly reported two-dimensional materials, such as single-element materials (Xenes) [36,37], and transition metal carbides or nitrides (MXenes) [38,39], were found to have great potential to realize low-threshold power mode-locked fiber lasers. This has created a new wave of interest among researchers in the search for new 2D materials with better properties.

$\text{Cr}_2\text{Si}_2\text{Te}_6$, a new layered material belonging to the hexatellurosilicate family [40], has received a lot of attention in the fields of sensors [41,42] and optical devices [43,44]. The atomic layers of $\text{Cr}_2\text{Si}_2\text{Te}_6$ are bound together by weak van der Waals forces, which also means that multilayered or few-layer 2D nanosheets can be obtained from their bulk-phase materials, by the liquid-phase exfoliation (LPE) method [45]. As a typical low-dimensional semiconductor material, the unique electronic, magnetic, and topological properties of $\text{Cr}_2\text{Si}_2\text{Te}_6$ have been demonstrated by using first-principle calculations and simulations, based on density functional theory [46,47]. In addition, $\text{Cr}_2\text{Si}_2\text{Te}_6$ has been used in a variety of applications, benefiting from its magnetic and electronic properties [48]. At the same time, $\text{Cr}_2\text{Si}_2\text{Te}_6$ has an indirect band gap value of ~0.6 eV, which makes it suitable for applications in near-infrared lasers [49]. Moreover, the ferromagnetism property of $\text{Cr}_2\text{Si}_2\text{Te}_6$ can exist not only in bulk, but also in single layers, which means that $\text{Cr}_2\text{Si}_2\text{Te}_6$ may have the possibility to create robust and single-layer ferromagnetic insulators. Researchers are also continuing to explore its curious properties, such as thermoelectric effect, superconductivity, and photovoltaic effect. However, there are few studies on $\text{Cr}_2\text{Si}_2\text{Te}_6$ -based optical modulators, especially in low-threshold and harmonic mode-locked fiber lasers. In 2021, Zhu et al. reported a large-energy Er-doped fiber laser, with a $\text{Cr}_2\text{Si}_2\text{Te}_6$ -based saturable absorber, the threshold was over 200 mW and the frequency of mode-locked operation was only 1.61 MHz. In 2022, based on $\text{Cr}_2\text{Si}_2\text{Te}_6$, Yang et al. reported a traditional soliton fiber laser whose threshold and frequency were 120 mW and 6.7 MHz.

In this work, a 15.1 mW low-threshold mode-locked fiber laser is demonstrated successfully. Such a low start-up threshold is mainly attributable to the low insertion loss and low saturation intensity of $\text{Cr}_2\text{Si}_2\text{Te}_6$ -based saturable absorber. The results indicate that the liquid-phase exfoliation (LPE) method is a useful and economical way to produce high-performance saturable absorbers. Besides, multiple high-order harmonics, from the fundamental frequency (12.6 MHz) to the 49th-order harmonic (617.6 MHz), mode-locked operations are recorded. All of these prove the excellent potential of $\text{Cr}_2\text{Si}_2\text{Te}_6$ in exploring the soliton dynamics, harmonic mode locking, and other nonlinear optical effects in fiber lasers, as optical modulators.

2. Preparation and Characteristics of the $\text{Cr}_2\text{Si}_2\text{Te}_6$ -Based SA

The $\text{Cr}_2\text{Si}_2\text{Te}_6$ -based SA was prepared by the commonly adopted LPE method, considering the air stability property of $\text{Cr}_2\text{Si}_2\text{Te}_6$. The preparation process is shown in Figure 1. $\text{Cr}_2\text{Si}_2\text{Te}_6$ bulk (20 mg) was ground into powder and mixed with 50 mL 99% ethanol, in the first step. After 24 h of soaking, the mixture was placed in an ultrasonic cleaner for 48 h, in order to obtain $\text{Cr}_2\text{Si}_2\text{Te}_6$ nanosheets. Then, 10 mL of the solution was taken and mixed with 10 mL 4 wt% polyvinyl alcohol (PVA) solution. This 20 mL solution was then put in the ultrasonic cleaner for 6 h. After this, the $\text{Cr}_2\text{Si}_2\text{Te}_6$ -PVA solution was pipetted onto a clean glass sheet. The glass sheet was then rotated at a constant speed. The solution formed a $\text{Cr}_2\text{Si}_2\text{Te}_6$ -PVA film after ~24 h of natural drying. Finally, the $\text{Cr}_2\text{Si}_2\text{Te}_6$ -based SA was prepared successfully by cutting the film into a sheet of appropriate size, and clamping the film between the end faces of two optical fiber patch cables.

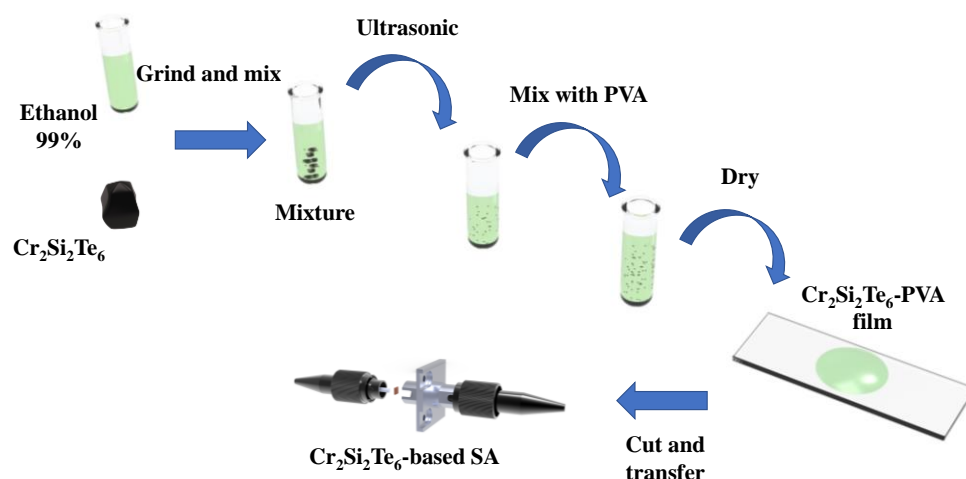


Figure 1. Preparation process of the $\text{Cr}_2\text{Si}_2\text{Te}_6$ -based SA.

In order to test the purity and physicochemical properties of the prepared $\text{Cr}_2\text{Si}_2\text{Te}_6$ nanosheets, we characterized the material as follows. Figure 2a shows the picture from a scanning electron microscope (SEM), at a resolution of 5 μm . An obvious layered structure can be observed and the thickness of one $\text{Cr}_2\text{Si}_2\text{Te}_6$ sheet is about 14 μm . The $\text{Cr}_2\text{Si}_2\text{Te}_6$ spectrum from an energy dispersive spectrometer (EDS) is given in Figure 2b, in which the ratios of Cr, Si, and Te are 21.75%, 15.63%, and 62.67%, respectively, which correspond well with 1:1:3 in the chemical formula of $\text{Cr}_2\text{Si}_2\text{Te}_6$. In addition, we used Raman spectroscopy to test the structural properties. Two strong Raman peaks were located at 120 cm^{-1} , 140 cm^{-1} , which correspond to the Eg_3 and Ag_3 modes of $\text{Cr}_2\text{Si}_2\text{Te}_6$ [50]. The images from the high-resolution transmission electron microscope (HRTEM), shown in Figure 2d–f, exhibit an obvious layered structure, and clear crystal lattices, with a d-spacing of ~ 0.25 nm, can be observed, which indicates the prepared $\text{Cr}_2\text{Si}_2\text{Te}_6$ nanosheets have excellent crystallinity properties. In addition, a femtosecond laser was used to test the nonlinear saturable absorption properties of the homemade SA. The testing setup is shown in Figure 3a. The central wavelength, pulse width, and frequency of the femtosecond laser are 1565 nm, 348 fs, and

10.8 MHz, respectively. A variable optical amplifier (VOA) is used to adjust the input pulse's intensity. The input pulses are split into two beams through a 1:1 optical coupler (OC) and the SA is injected into one part of the OC. The output power of the two parts of the OC is recorded by a power meter (PM). The experimental data and fitting curve, fitted by

$$T(I) = 1 - T_{ns} - \Delta \exp\left(-\frac{I}{I_{sat}}\right) \quad (1)$$

are shown in Figure 3b. $T(I)$ is the transmission rate, T_{ns} is the non-saturable loss, Δ is the modulation depth, I is the input intensity, and I_{sat} is the saturation intensity. From the formula, the saturation intensity, non-saturable loss, and modulation depth can be calculated, which are 28.6 MW/cm^2 , 15.78%, and 10.7%, respectively.

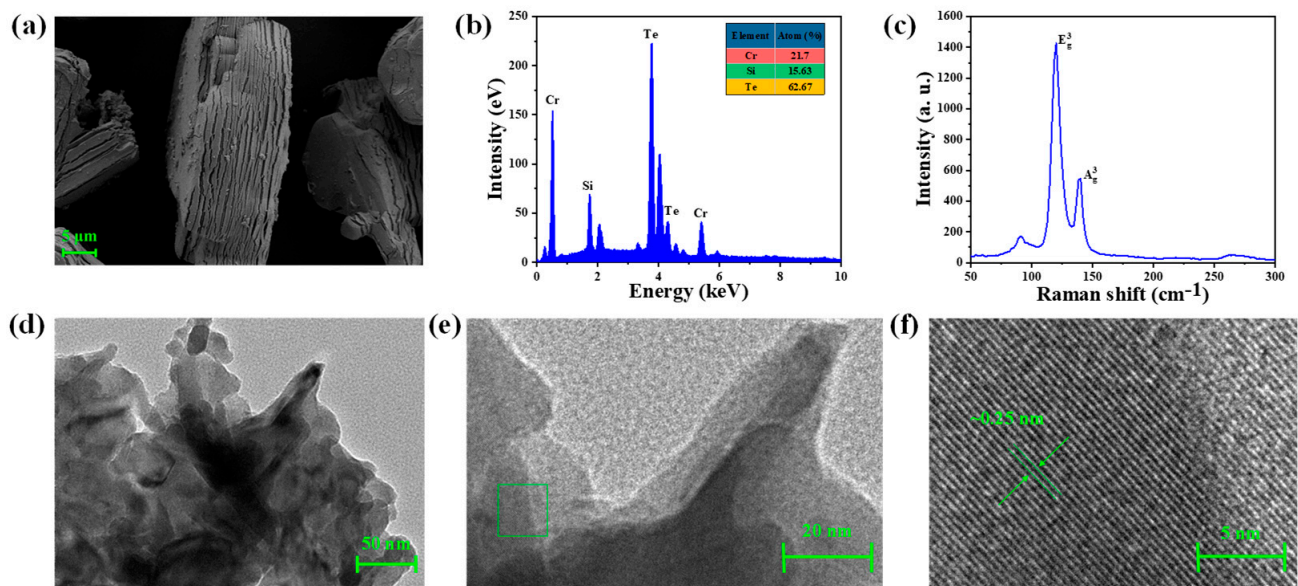


Figure 2. Characteristics of the $\text{Cr}_2\text{Si}_2\text{Te}_6$ nanosheets. (a) SEM image, (b) EDS spectrum, (c) Raman spectrum, (d–f) HRTEM images at different resolutions.

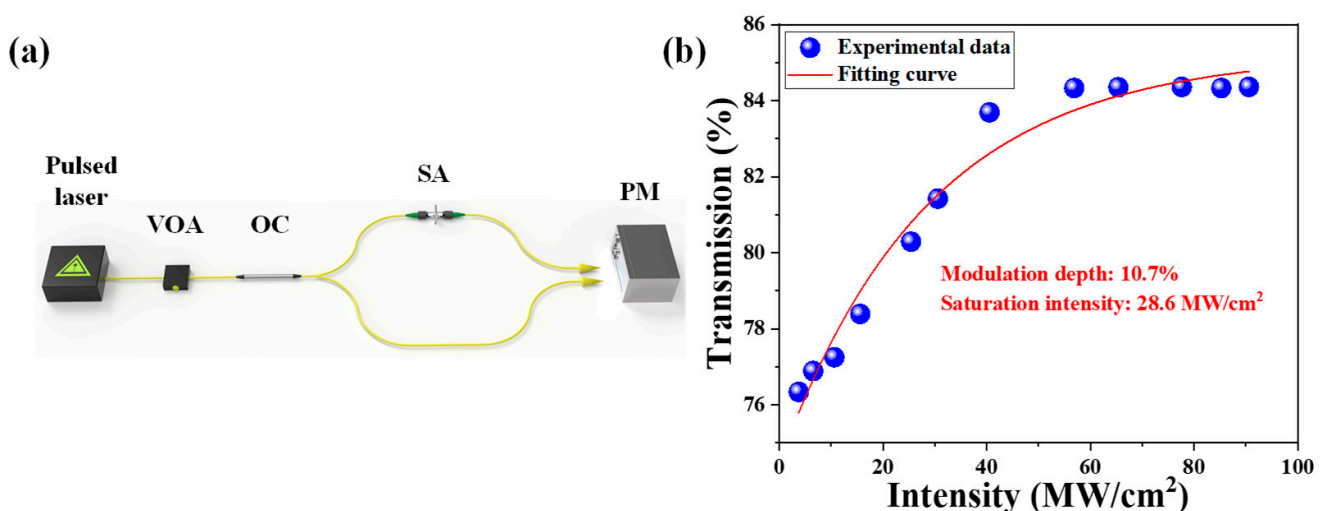


Figure 3. Nonlinear saturable absorption property of the $\text{Cr}_2\text{Si}_2\text{Te}_6$ -based SA. (a) The testing setup, (b) fitting curve.

3. Results and Discussion

A low-threshold mode-locked fiber laser, based on a $\text{Cr}_2\text{Si}_2\text{Te}_6$ SA, was constructed, with the structure shown in Figure 4. A 5 m Er-doped fiber (OFS-MP980) was utilized

as the gain medium, which was pumped by a 976 nm laser diode (976 nm/600 mW) through a 1550 nm/980 nm wavelength division multiplexer (WDM). Two polarization controllers (PCs) were used to adjust the birefringence and polarization state of the cavity. Besides, a polarization-independent isolator (PI-ISO) was used to ensure the unidirectional transmission of the laser. A part of a single-mode fiber was inserted to control the dispersion, gain, and loss of the cavity. In order to realize mode-locked operation, the $\text{Cr}_2\text{Si}_2\text{Te}_6$ SA was utilized as a mode locker. The operating condition of the fiber laser was recorded by an optical spectrum analyzer (Yokogawa, AQ6317B), a digital oscilloscope (Wavesurfer, 3054z) with a 2 GHz photo-detector, a radio frequency (RF) spectrum analyzer (Rohde & Schwarz, FPC1000), an auto-correlator (Femtochrome, FR-103XL), and an optical power meter through an optical coupler (OC, 10% output).

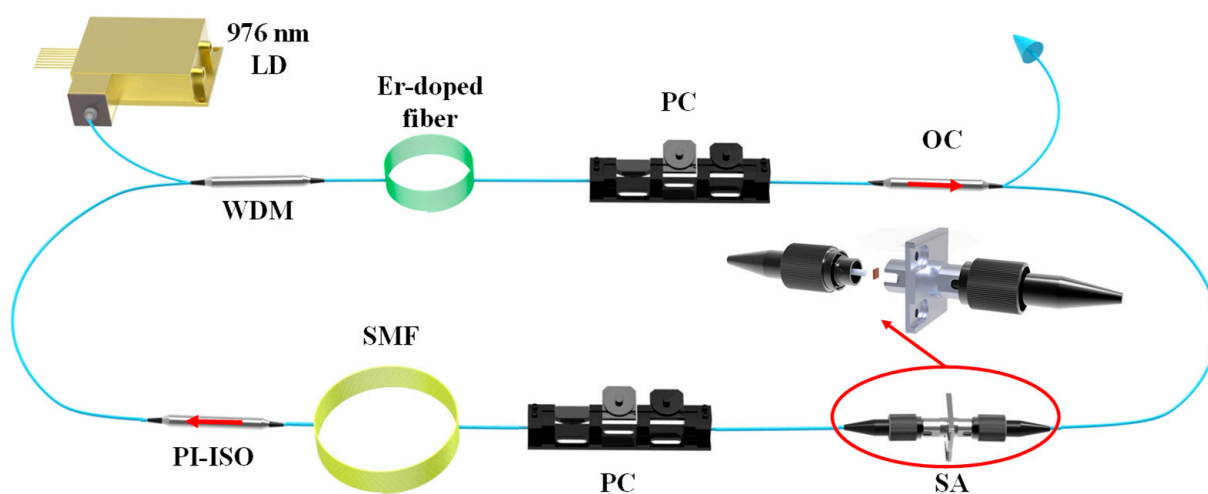


Figure 4. Structure of the low-threshold mode-locked fiber laser.

The output characteristics of the low-threshold mode-locked fiber laser are given in Figures 5–9. Figure 5a shows the tendency of the output power. Mode-locked operation under the fundamental (1st) frequency can be observed, as the pump power is lower than 24.4 mW. When the pump power is larger than 24.4 mW, a stable harmonic mode-locked state is obtained, where the repulsive and attractive forces between pulses are balanced [51]. In our work, the threshold of the fiber laser is as low as 15.1 mW, which is mainly attributable to the low insertion loss and low saturable intensity of the $\text{Cr}_2\text{Si}_2\text{Te}_6$ SA. Table 1 shows a comparison of mode-locked fiber lasers based on different 2D materials. The used $\text{Cr}_2\text{Si}_2\text{Te}_6$ SA has a relatively large modulation depth and a smaller saturation intensity. Especially, the non-saturable loss is much lower than most other saturable absorbers. Benefiting from these excellent nonlinear properties of the homemade $\text{Cr}_2\text{Si}_2\text{Te}_6$ SA, a lower start-up threshold and a higher signal-to-noise ratio (SNR) are realized in our work. The pulse trains and optical spectrum under the fundamental frequency (1st), are shown in Figure 5b,c. The fundamental frequency is 12.61 MHz, corresponding to the pulse interval of 79.3 ns. The center wavelength is located at 1556.4 nm, and there is a small peak caused by the continuous wavelength (CW) component, located at 1531.3 nm. Figure 5d exhibits the trend of the order of harmonic and the pulse width changing with pump power, in which the order of harmonic increases from the fundamental frequency to the 22nd harmonic, while the pulse width stays around 1.6 ps. Besides, the shortest pulse width recorded in our work was 1.4 ps, corresponding to the 15th harmonic, when the pump power was 86 mW. The auto-correlator trace of the 15th harmonic pulse is shown in Figure 5e, and the corresponding optical spectrum with the full width of half maximum (FWHM), of 3.6 nm, is given in Figure 5f.

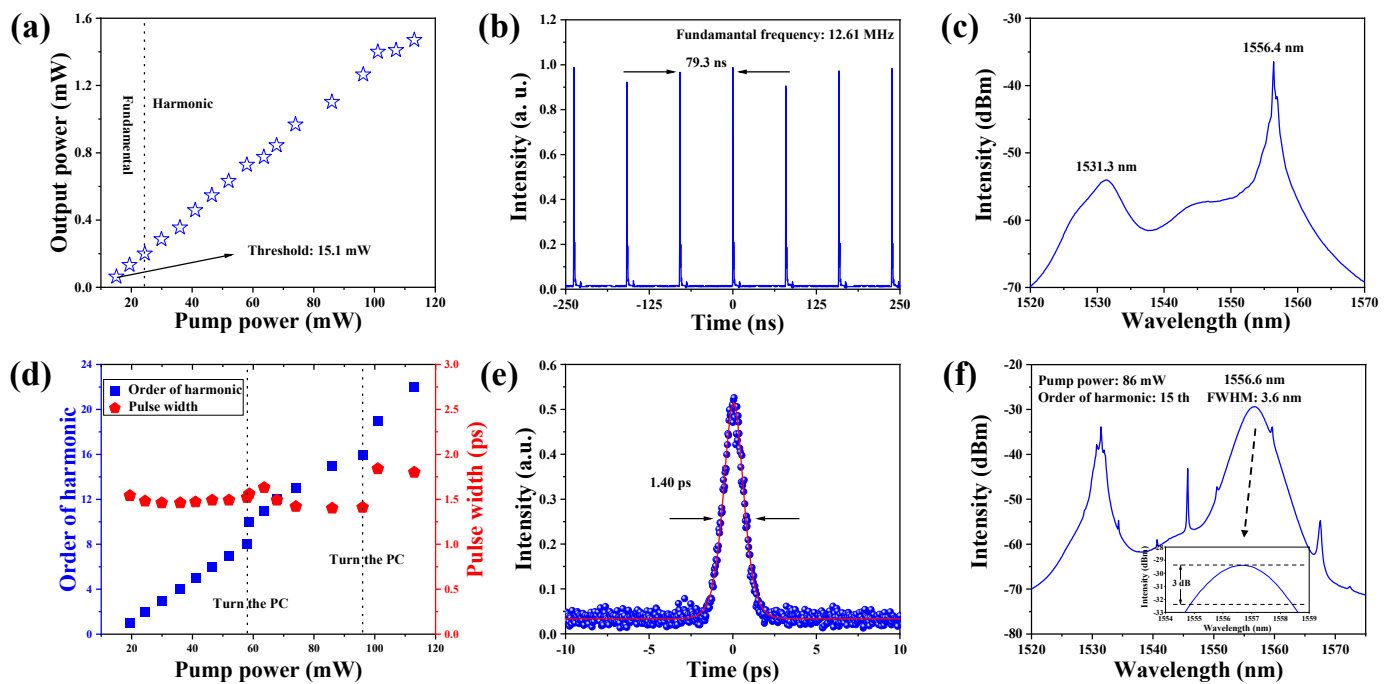


Figure 5. (a) Tendency of output power, (b) pulse trains under fundamental frequency, (c) optical spectrum under fundamental frequency, (d) trend of the order of harmonic and the pulse width changing with pump power, (e) auto-correlator trace of 15th harmonic pulse, (f) optical spectrum of 15th harmonic pulse.

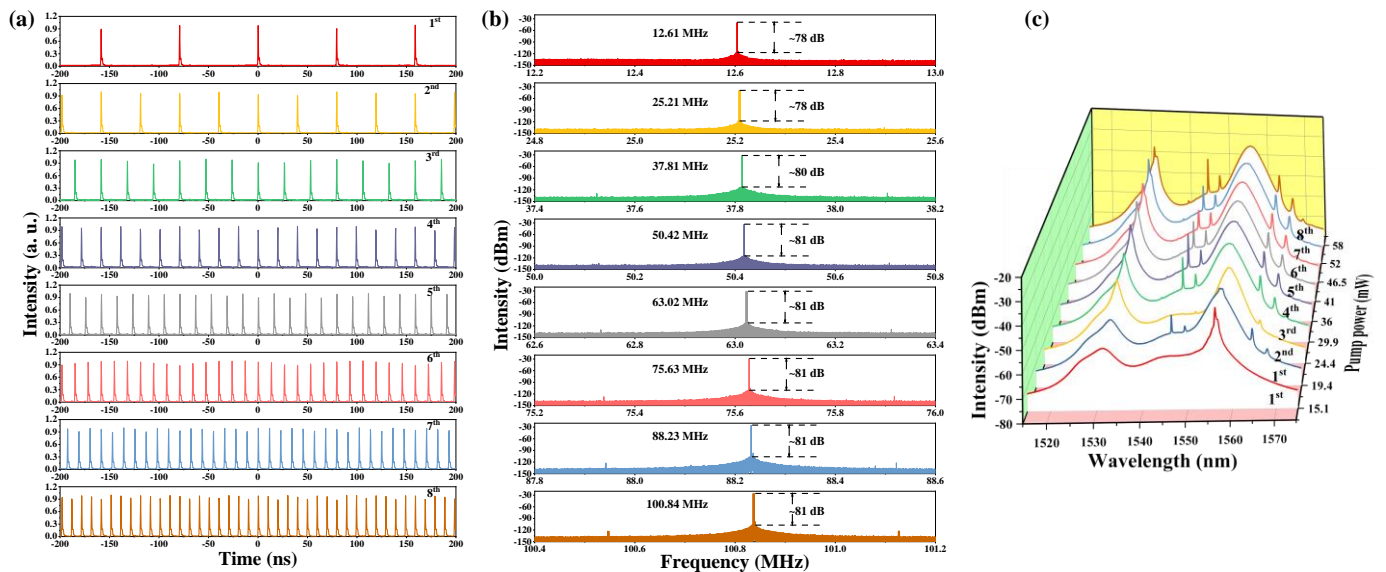


Figure 6. (a) Pulse trains from 1st–8th, (b) corresponding RF spectra, (c) changing trend of the optical spectra of the harmonic order from 1st–8th.

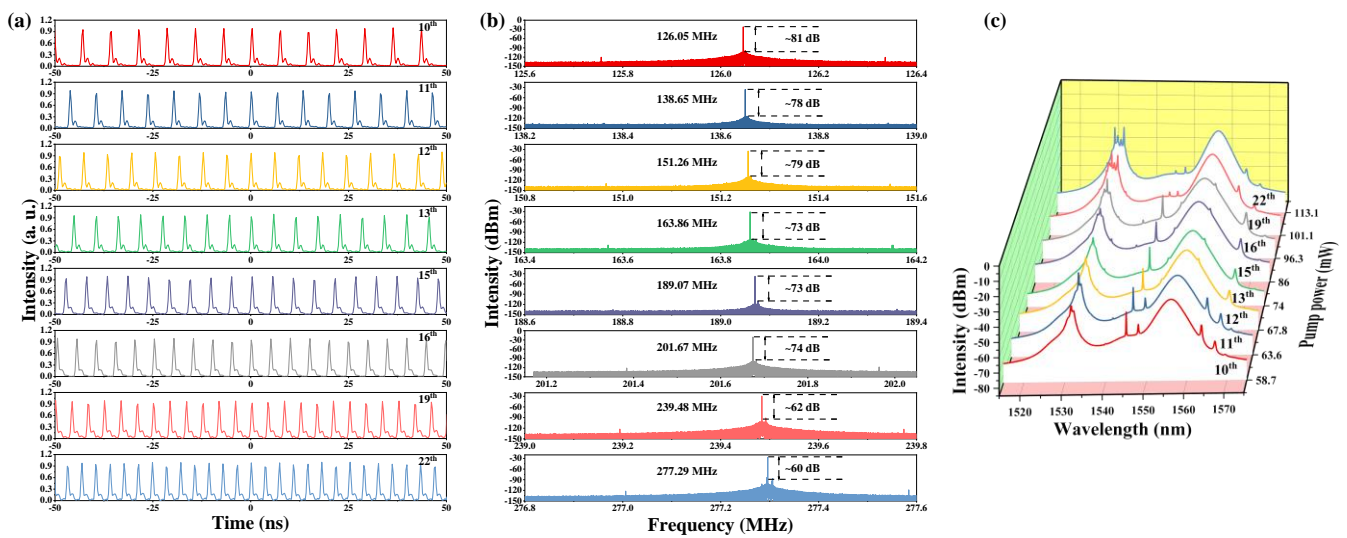


Figure 7. (a) Pulse trains from 10th–22nd, (b) corresponding RF spectra, (c) changing trend of the optical spectra of the harmonic order from 10th–22nd.

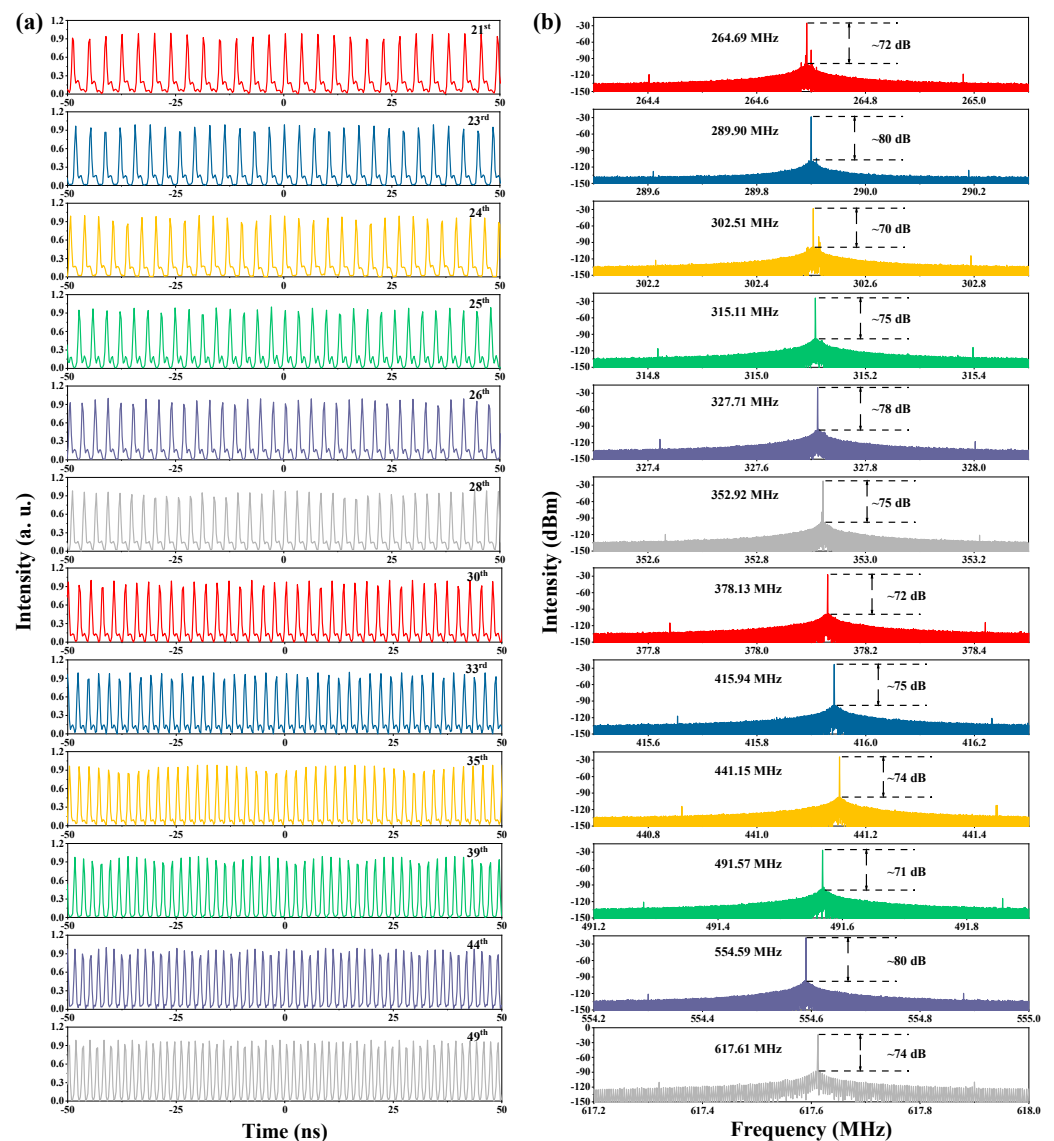


Figure 8. (a) Pulse trains from 21st–49th, (b) corresponding RF spectra.

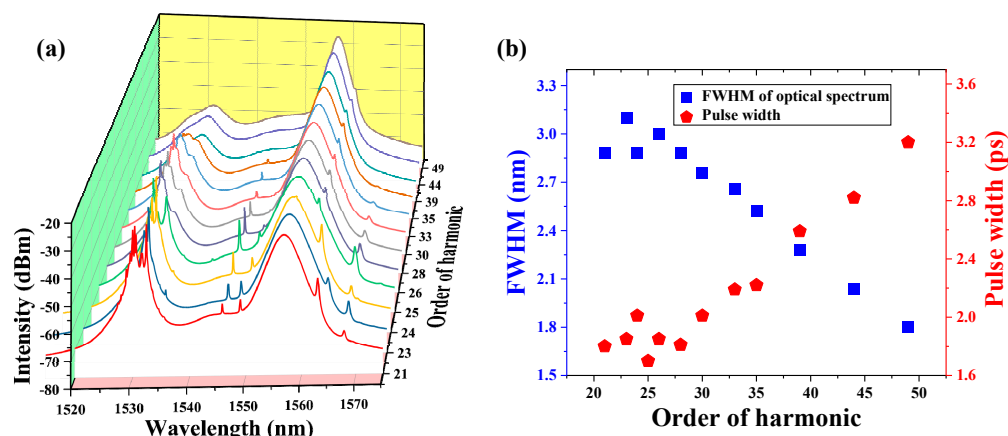


Figure 9. (a) Changing trend of the optical spectra of the harmonic order from 21st–49th, (b) changing trend of the FWHM and pulse width with the order of harmonics.

Table 1. Comparison of threshold of 1.5 μm mode-locked fiber lasers based on different 2D materials.

Materials	Preparation Method	MD (%)	SI (MW/cm^2)	NSL (%)	SNR (dB)	Threshold (mW)	Ref.
Graphene	CVD	2.7	-	-	64	47	[52]
	ME	3.6	0.08	44.2	70	38	[53]
Bi_2Te_3	LPE	4.8	-	73.4	60	80	[54]
Bi_2Se_3	Polyol	98	$0.49 \text{ GW}/\text{cm}^2$	-	-	65	[55]
Sb_2Te_3	LPE	3.9	106	87	74	44	[56]
BP	ME	0.6	-	-	65	80	[57]
	LPE	9	25	-	50	30	[58]
WS_2	PLD	7.8	189	25.7	64	65	[59]
MoS_2	MSD	19.48	4.137	38.53	75	40	[60]
WSe_2	LPE	0.5	-	47.2	-	35	[61]
MoSe_2	LPE	0.8	-	52	52	30.7	[62]
$\text{Ti}_3\text{C}_2\text{T}_x$	LPE	0.96	256.9	73.5	71	146	[63]
Antimonene	LPE	9	$1.3 \text{ GW}/\text{cm}^2$	9	-	130	[36]
Bismuthene	LPE	2.03	30	82.5	55	153	[64]
Tellurene	LPE	5.06	34.3	58.6	55	85	[21]
$\text{Cr}_2\text{Si}_2\text{Te}_6$	LPE	10.7	28.6	15.78	81	15.1	ours

MD: modulation depth, SI: saturation intensity, CVD: chemical vapor deposition, ME: mechanical stripping, PLD: pulse laser deposition, MSD: magnetron sputtering deposition, NSL: non-saturable loss.

Under a large pump power, multiple pulses will be aroused in the laser cavity, with appropriate net dispersion and strong nonlinear effects [65]. The attractive force between these multiple pulses will lead to the generation of soliton rain and bound state [66,67]. In contrast, the repulsive force between them will drive them away from each other, in a regular or irregular arrangement [51]. The generation of harmonic mode locking has been proved to be a result of the interaction of multiple pulses under gain depletion and recovery mechanism, the non-soliton component of radiation, and the acoustic wave effect [68–70]. In our work, when the pump power increases from 15.1 mW to 58 mW, the order of harmonic varies from 1st to 8th continuously. The pulse trains of the 1st–8th harmonics are given in Figure 6a. The corresponding RF spectra are exhibited in Figure 6b, in which the SNR is around 80 dB, which indicates that the fiber laser operates stably under both the fundamental frequency and harmonic states. Besides, the changing trend of optical spectra can be observed in Figure 6c. The intensity of the peak located at 1531.3 nm clearly increases with the increase in the pump power, and there is a tendency for it to split.

The pulse trains become a little unstable when the pump power is over 58 mW. So one of the PCs was turned slightly and we obtained the 10th harmonic pulse, under the pump power of 58.7 mW. The pulse trains of the 10th–22nd harmonics are given in Figure 7a, and the corresponding RF spectra are exhibited in Figure 7b. With the increase in the order, there

is a marked decline in the SNR. But all of them are larger than 60 dB, which indicates the operating state of our fiber laser is stable enough. The optical spectra corresponding to the 10th–22nd harmonics can be observed in Figure 7c. The intensity of the peak of 1531.3 nm is equal to that of 1556.6 nm, and obvious splits can be observed in the higher-order harmonic. At the time, the Kelly sidebands have a trend of decline with the increase in the order of harmonics.

A higher order of harmonic pulses from the 21st to 49th can also be recorded by adjusting the PC, under the pump power of 113.1 mW. Figure 8a shows the pulse trains and Figure 8b gives the corresponding RF spectra. The SNR can be maintained between 70 dB and 80 dB, illustrating the stable operating state of the high-order harmonic. Different from the varying trend of the optical spectra, when the order is lower than the 22nd, the peak at 1531.3 nm changes in a completely opposite trend, with an increase in the order of the harmonic, which can be observed in Figure 9a. Besides, there is an obvious narrowing process of the FWHM of the optical spectra from 3.1 nm to 1.8 nm, which can be seen in Figure 9b. In addition, the pulse width increases from 1.7–3.2 ps with the increase in the order of harmonics.

When the pump power is higher than 113.1 mW, chaotic pulse generation can also be observed, but no matter how we adjust the PC, no stable pulse sequence is obtained. This is mainly limited by the deficiency of the intracavity nonlinear effect and dispersion [65].

4. Conclusions

A 15.1-mW low-threshold mode-locked fiber laser is demonstrated successfully in this work. Such a low start-up threshold is mainly attributable to the $\text{Cr}_2\text{Si}_2\text{Te}_6$ -based saturable absorber, which has low insertion loss and low saturation intensity. Besides, multiple high-order harmonics, from the fundamental frequency to 49th-order harmonic, mode-locked operations are recorded. The results indicate that the liquid-phase exfoliation method is a useful and economical way to produce high-performance saturable absorbers, and prove the excellent potential of $\text{Cr}_2\text{Si}_2\text{Te}_6$ in exploring the soliton dynamics, harmonic mode locking, and other nonlinear optical effects in fiber lasers, as an optical modulator.

Author Contributions: Writing—original draft preparation, N.X. and X.S.; conceptualization, S.S., F.Y. and W.F.; investigation, S.S.; project administration, H.Z. and D.L.; funding acquisition, H.Z. and D.L. All authors have read and agreed to the published version of the manuscript.

Funding: This work was supported by the National Natural Science Foundation of China (Grant nos. 61971271, 62271294), the Major Program of Shandong Province Natural Science Foundation (ZR2022ZD16), the Shandong Province Major Technological Innovation Project (2022CXGC020507, 2022CXGC010502, 2022CXGC020505), the Jinan City-School Integration Development Strategy Project (JNSX2021023), and supported by “Opening Foundation of Shandong Provincial Key Laboratory of Laser Technology and Application”.

Data Availability Statement: Data underlying the results presented in this paper are not publicly available at this time but may be obtained from the authors upon reasonable request.

Conflicts of Interest: The authors declare no conflict of interest.

References

1. Turunen, M.; Brotons-Gisbert, M.; Dai, Y.Y.; Wang, Y.D.; Scerri, E.; Bonato, C.; Jöns, K.D.; Sun, Z.P.; Gerardot, B.D. Quantum photonics with layered 2D materials. *Nat. Rev. Phys.* **2022**, *4*, 219–236.
2. Zeng, L.H.; Wu, D.; Jie, J.S.; Ren, X.Y.; Hu, X.; Lau, S.P.; Chai, Y.; Tsang, Y.H. Van der Waals epitaxial growth of mosaic-like 2D platinum ditelluride layers for room-temperature mid-infrared photodetection up to 10.6 μm . *Adv. Mater.* **2020**, *32*, 2004412. [[CrossRef](#)] [[PubMed](#)]
3. Wu, D.; Guo, J.W.; Wang, C.Q.; Ren, X.Y.; Chen, Y.S.; Lin, P.; Zeng, L.H.; Shi, Z.F.; Li, X.J.; Shan, C.X.; et al. Ultrabroadband and high-detectivity photodetector based on WS_2/Ge heterojunction through defect engineering and interface passivation. *ACS Nano* **2021**, *15*, 10119–10129. [[CrossRef](#)]
4. Ge, X.X.; Xia, Z.H.; Guo, S.J. Recent advances on black phosphorus for biomedicine and biosensing. *Adv. Funct. Mater.* **2019**, *29*, 1900318. [[CrossRef](#)]

5. Glavin, N.R.; Rao, R.; Varshney, V.; Bianco, E.; Apte, A.; Roy, A.; Ringe, E.; Ajayan, P.M. Emerging applications of elemental 2D materials. *Adv. Mater.* **2020**, *32*, 1904302. [\[CrossRef\]](#)
6. Wu, D.; Xu, M.M.; Zeng, L.H.; Shi, Z.F.; Tian, Y.Z.; Li, X.J.; Shan, C.X.; Jie, J.S. In Situ Fabrication of PdSe₂/GaN Schottky Junction for Polarization-Sensitive Ultraviolet Photodetection with High Dichroic Ratio. *ACS Nano* **2022**, *16*, 5545–5555. [\[CrossRef\]](#) [\[PubMed\]](#)
7. Zeng, L.H.; Wu, D.; Lin, S.H.; Xie, C.; Yuan, H.Y.; Lu, W.; Lau, S.P.; Chai, Y.; Luo, L.B.; Li, Z.J.; et al. Controlled synthesis of 2D palladium diselenide for sensitive photodetector applications. *Adv. Funct. Mater.* **2019**, *29*, 1806878. [\[CrossRef\]](#)
8. Liu, W.J.; Liu, M.L.; Liu, X.M.; Wang, X.T.; Deng, H.X.; Lei, M.; Wei, Z.M.; Wei, Z.Y. Recent advances of 2D materials in nonlinear photonics and fiber lasers. *Adv. Opt. Mater.* **2020**, *8*, 1901631. [\[CrossRef\]](#)
9. He, J.S.; Tao, L.L.; Zhang, H.; Zhou, B.; Li, J.B. Emerging 2D materials beyond graphene for ultrashort pulse generation in fiber lasers. *Nanoscale* **2019**, *11*, 2577–2593. [\[CrossRef\]](#)
10. Yu, S.L.; Wu, X.Q.; Wang, Y.P.; Guo, X.; Tong, L.M. 2D materials for optical modulation: Challenges and opportunities. *Adv. Mater.* **2017**, *29*, 1606128. [\[CrossRef\]](#)
11. Fu, B.; Sun, J.X.; Wang, G.; Shang, C.; Ma, Y.X.; Ma, J.G.; Xu, L.J.; Scardaci, V. Solution-processed two-dimensional materials for ultrafast fiber lasers. *Nanophotonics* **2020**, *9*, 2169–2189. [\[CrossRef\]](#)
12. Yamashita, S. Nonlinear optics in carbon nanotube, graphene, and related 2D materials. *APL Photonics* **2019**, *4*, 034301. [\[CrossRef\]](#)
13. Zhang, H.N.; Sun, S.; Shang, X.X.; Guo, B.; Li, X.H.; Chen, X.H.; Jiang, S.Z.; Zhang, H.; Ågren, H.; Zhang, W.F.; et al. Ultrafast photonics applications of emerging 2D-Xenes beyond graphene. *Nanophotonics* **2022**, *11*, 1261–1284. [\[CrossRef\]](#)
14. Jiang, T.; Yin, K.; Wang, C.; You, J.; Ouyang, H.; Miao, R.L.; Zhang, C.X.; Wei, K.; Li, H.; Chen, H.T.; et al. Ultrafast fiber lasers mode-locked by two-dimensional materials: Review and prospect. *Photonics Res.* **2020**, *8*, 78–90. [\[CrossRef\]](#)
15. Nakazawa, M.; Yoshida, E.; Kimura, Y. Low threshold, 290 fs erbium-doped fiber laser with a nonlinear amplifying loop mirror pumped by InGaAsP laser diodes. *Appl. Phys. Lett.* **1991**, *59*, 2073–2075. [\[CrossRef\]](#)
16. Mondal, S.; Ganguly, R.; Mondal, K. Topological Insulators: An In-Depth Review of Their Use in Modelocked Fiber Lasers. *Ann. Phys.* **2021**, *533*, 2000564. [\[CrossRef\]](#)
17. Yusoff, N.M.; Abdullah, C.A.C.; Hadi, M.A.; Ng, E.K.; Lee, H.K.; Abidin, N.Z.; Rosli, N.S.; Mahdi, M.A. Low threshold Q-switched fiber laser incorporating titanium dioxide saturable absorber from waste material. *Optik* **2020**, *218*, 164998. [\[CrossRef\]](#)
18. Lü, B.; Rudolph, W.; Weber, H. Statistics of mode-locking threshold. *Opt. Commun.* **1985**, *53*, 203–209. [\[CrossRef\]](#)
19. Li, L.; Pang, L.H.; Zhao, Q.Y.; Wang, Y.G.; Liu, W.J. Niobium disulfide as a new saturable absorber for an ultrafast fiber laser. *Nanoscale* **2020**, *12*, 4537–4543. [\[CrossRef\]](#)
20. Sun, S.; Yang, F.H.; Sui, Z.Q.; Zhu, M.X.; Chen, S.; Wang, Y.J.; Hong, Z.F.; Zhang, W.F.; Fu, S.G.; Chen, X.H.; et al. Demonstration of passively Q-switched and mode-locked operations through dispersion control in Er-doped fiber lasers with a cylindrite-based saturable absorber. *J. Lumin.* **2022**, *250*, 119064. [\[CrossRef\]](#)
21. Xu, N.N.; Ma, P.F.; Fu, S.G.; Shang, X.X.; Jiang, S.Z.; Wang, S.Y.; Li, D.W.; Zhang, H.N. Tellurene-based saturable absorber to demonstrate large-energy dissipative soliton and noise-like pulse generations. *Nanophotonics* **2020**, *9*, 2783–2795. [\[CrossRef\]](#)
22. Gao, Q.; Yang, H.; Hu, C.; He, Z.W.; Lu, H.; Zhang, W.D.; Mao, D.; Mei, T.; Zhao, J.L. Physical vapor deposition of large-scale PbSe films and its applications in pulsed fiber lasers. *Nanophotonics* **2020**, *9*, 2367–2375. [\[CrossRef\]](#)
23. Liu, W.J.; Liu, M.L.; Chen, X.; Shen, T.; Lei, M.; Guo, J.G.; Deng, H.X.; Zhang, W.; Dai, C.Q.; Zhang, X.F.; et al. Ultrafast photonics of two dimensional AuTe₂Se_{4/3} in fiber lasers. *Commun. Phys.* **2020**, *3*, 15. [\[CrossRef\]](#)
24. Liu, M.L.; Wu, H.B.; Liu, X.M.; Wang, Y.R.; Lei, M.; Liu, W.J.; Guo, W.; Wei, Z.Y. Optical properties and applications of SnS₂ SAs with different thickness. *Opto-Electron. Adv.* **2021**, *4*, 200029-1. [\[CrossRef\]](#)
25. Yan, P.G.; Lin, R.Y.; Ruan, S.C.; Liu, A.J.; Chen, H.; Zheng, Y.Q.; Chen, S.F.; Guo, C.Y.; Hu, J.G. A practical topological insulator saturable absorber for mode-locked fiber laser. *Sci. Rep.* **2015**, *5*, 8690. [\[CrossRef\]](#)
26. Wang, Z.H.; Li, C.Y.; Ye, J.W.; Wang, Z.; Liu, Y.G. Generation of harmonic mode-locking of bound solitons in the ultrafast fiber laser with Sb₂Te₃ saturable absorber on microfiber. *Laser. Phys. Lett.* **2019**, *16*, 025103. [\[CrossRef\]](#)
27. Liu, W.J.; Xiong, X.L.; Liu, M.L.; Xing, X.W.; Chen, H.L.; Ye, H.; Han, J.F.; Wei, Z.Y. Bi₄Br₄-based saturable absorber with robustness at high power for ultrafast photonic device. *Appl. Phys. Lett.* **2022**, *120*, 053108. [\[CrossRef\]](#)
28. Yin, K.; Zhang, B.; Li, L.; Jiang, T.; Zhou, X.F.; Hou, J. Soliton mode-locked fiber laser based on topological insulator Bi₂Te₃ nanosheets at 2 μm. *Photonics Res.* **2015**, *3*, 72–76. [\[CrossRef\]](#)
29. Liu, X.; Gao, Q.; Zheng, Y.; Mao, D.; Zhao, J.L. Recent progress of pulsed fiber lasers based on transition-metal dichalcogenides and black phosphorus saturable absorbers. *Nanophotonics* **2020**, *9*, 2215–2231. [\[CrossRef\]](#)
30. Zhang, M.; Wu, Q.; Zhang, F.; Chen, L.L.; Jin, X.X.; Hu, Y.W.; Zheng, Z.; Zhang, H. 2D black phosphorus saturable absorbers for ultrafast photonics. *Adv. Opt. Mater.* **2019**, *7*, 1800224. [\[CrossRef\]](#)
31. Yu, H.; Zheng, X.; Yin, K.; Chen, X.A.; Jiang, T. Thulium/holmium-doped fiber laser passively mode locked by black phosphorus nanoplatelets-based saturable absorber. *Appl. Opt.* **2015**, *54*, 10290–10294. [\[CrossRef\]](#) [\[PubMed\]](#)
32. Xu, N.N.; Wang, H.F.; Zhang, H.N.; Guo, L.G.; Shang, X.X.; Jiang, S.Z.; Li, D.W. Palladium diselenide as a direct absorption saturable absorber for ultrafast mode-locked operations: From all anomalous dispersion to all normal dispersion. *Nanophotonics* **2020**, *9*, 4295–4306. [\[CrossRef\]](#)
33. Shang, X.X.; Xu, N.N.; Zhang, H.N.; Li, D.W. Nonlinear photoresponse of high damage threshold titanium disulfide nanocrystals for Q-switched pulse generation. *Opt. Laser. Technol.* **2022**, *151*, 107988. [\[CrossRef\]](#)

34. Lee, J.; Koo, J.; Lee, J.; Jhon, Y.M.; Lee, J.H. All-fiberized, femtosecond laser at 1912 nm using a bulk-like MoSe₂ saturable absorber. *Opt. Mater. Express* **2017**, *7*, 2968–2979. [[CrossRef](#)]
35. Wu, K.; Zhang, X.Y.; Wang, J.; Li, X.; Chen, J.P. WS₂ as a saturable absorber for ultrafast photonic applications of mode-locked and Q-switched lasers. *Opt. Express* **2015**, *23*, 11453–11461. [[CrossRef](#)]
36. Liu, G.W.; Zhang, F.; Wu, T.G.; Li, Z.W.; Zhang, W.F.; Han, K.Z.; Xing, F.; Man, Z.S.; Ge, X.L.; Fu, S.G. Single- and dual-wavelength passively mode-locked erbium-doped fiber laser based on antimonene saturable absorber. *IEEE Photon. J.* **2019**, *11*, 1–11. [[CrossRef](#)]
37. Guo, B.; Wang, S.H.; Wu, Z.X.; Wang, Z.X.; Wang, D.H.; Huang, H.; Zhang, F.; Ge, Y.Q.; Zhang, H. Sub-200 fs soliton mode-locked fiber laser based on bismuthene saturable absorber. *Opt. Express* **2018**, *26*, 22750–22760. [[CrossRef](#)]
38. Huang, W.C.; Ma, C.Y.; Li, C.; Zhang, Y.; Hu, L.P.; Chen, T.T.; Tang, Y.F.; Jun, J.F.; Zhang, H. Highly stable MXene (V₂CT_x)-based harmonic pulse generation. *Nanophotonics* **2020**, *9*, 2577–2585. [[CrossRef](#)]
39. Gao, L.F.; Ma, C.Y.; Wei, S.R.; Kuklin, A.V.; Zhang, H.; Ågren, H. Applications of few-layer Nb₂C MXene: Narrow-band photodetectors and femtosecond mode-locked fiber lasers. *ACS Nano* **2021**, *15*, 954–965. [[CrossRef](#)]
40. Ouvrard, G.; Sandre, E.; Brec, R. Synthesis and crystal structure of a new layered phase: The chromium hexatellurosulfate Cr₂Si₂Te₆. *J. Solid State Chem.* **1988**, *73*, 27–32. [[CrossRef](#)]
41. Liu, X.; Wang, Z.Y.; Liu, D.Y.; Zou, L.J. Enhancement of Curie temperature and reorientation of spin in doped Cr₂Si₂Te₆. *AIP Adv.* **2021**, *11*, 095002. [[CrossRef](#)]
42. Hong, Z.F.; Jiang, X.W.; Zhang, M.X.; Zhang, H.N.; Liu, X.J. High Power and Large-Energy Pulse Generation in an Erbium-Doped Fiber Laser by a Ferromagnetic Insulator-Cr₂Si₂Te₆ Saturable Absorber. *Nanomaterials* **2022**, *12*, 564. [[CrossRef](#)] [[PubMed](#)]
43. Xu, N.N.; Sun, S.; Shang, X.X.; Zhang, H.N.; Li, D.W. Harmonic and fundamental-frequency mode-locked operations in an Er-doped fiber laser using a Cr₂Si₂Te₆-based saturable absorber. *Opt. Mater. Express* **2022**, *12*, 166–173. [[CrossRef](#)]
44. Liu, Y.; Susilo, R.A.; Lee, Y.; Abeykoon, A.M.; Tong, X.; Hu, Z.X.; Stavitski, E.; Attenkofer, K.; Ke, L.Q.; Chen, B.; et al. Short-Range Crystalline Order-Tuned Conductivity in Cr₂Si₂Te₆ van der Waals Magnetic Crystals. *ACS Nano* **2022**, *16*, 13134–13143. [[CrossRef](#)]
45. Zhao, H.D.; Ni, Y.F.; Hu, B.; Selter, S.; Aswartham, S.; Zhang, Y.; Büchner, B.; Schlottmann, P.; Cao, G. Mechanical control of physical properties in the van der Waals ferromagnet Cr₂Ge₂Te₆ via application of electric current. *arXiv* **2022**, arXiv:2201.08509. [[CrossRef](#)]
46. Kang, S.; Kang, S.; Kim, H.S.; Yu, J. Field-controlled quantum anomalous Hall effect in electron-doped CrSiTe₃ monolayer: A first-principles prediction. *arXiv* **2022**, arXiv:2208.02997.
47. Cai, W.P.; Sun, H.L.; Xia, W.; Wu, C.W.; Liu, Y.; Liu, H.; Gong, Y.; Yao, D.X.; Guo, Y.F.; Wang, M. Pressure-induced superconductivity and structural transition in ferromagnetic CrSiTe₃. *Phys. Rev. B* **2020**, *102*, 144525. [[CrossRef](#)]
48. Baranova, M.S.; Hvazdouski, D.C.; Skachkova, V.A.; Stempitsky, V.R.; Danilyuk, A.L. Magnetic interactions in Cr₂Ge₂Te₆ and Cr₂Si₂Te₆ monolayers: Ab initio study. *Mater. Today Proc.* **2020**, *20*, 342–347. [[CrossRef](#)]
49. Carteaux, V.; Brunet, D.; Ouvrard, G.; Andre, G. Crystallographic, magnetic and electronic structures of a new layered ferromagnetic compound Cr₂Ge₂Te₆. *J. Phys. Condens. Matter.* **1995**, *7*, 69. [[CrossRef](#)]
50. Milosavljević, A.; Šolajić, A.; Pešić, J.; Liu, Y.; Petrović, C.; Lazarević, N.; Popović, Z.V. Evidence of spin-phonon coupling in CrSiTe₃. *Phys. Rev. B* **2018**, *98*, 104306. [[CrossRef](#)]
51. Liu, X.; Pang, M. Revealing the buildup dynamics of harmonic mode-locking states in ultrafast lasers. *Laser. Photonics Rev.* **2019**, *13*, 1800333. [[CrossRef](#)]
52. Fu, B.; Hua, Y.; Xiao, X.S.; Zhu, H.W.; Sun, Z.P.; Yang, C.Y. Broadband graphene saturable absorber for pulsed fiber lasers at 1, 1.5, and 2 μm. *IEEE J. Sel. Top. Quantum Electron.* **2014**, *20*, 411–415.
53. Sobon, G.; Sotor, J.; Abramski, K.M. All-polarization maintaining femtosecond Er-doped fiber laser mode-locked by graphene saturable absorber. *Laser. Phys. Lett.* **2012**, *9*, 581. [[CrossRef](#)]
54. Duan, L.N.; Wang, Y.G.; Xu, C.W.; Li, L.; Wang, Y.S. Passively Harmonic Mode-Locked Fiber Laser With a High Signal-to-Noise Ratio via Evanescent-Light Deposition of Bismuth Telluride Bi₂Te₃ Topological Insulator Based Saturable Absorber. *IEEE Photon. J.* **2015**, *7*, 1–7. [[CrossRef](#)]
55. Zhao, C.J.; Zou, Y.H.; Chen, Y.; Wang, Z.T.; Lu, S.B.; Zhang, H.; Wen, S.C.; Tang, D.Y. Wavelength-tunable picosecond soliton fiber laser with topological insulator: Bi₂Se₃ as a mode locker. *Opt. Express* **2012**, *20*, 27888–27895. [[CrossRef](#)]
56. Boguslawski, J.; Sotor, J.; Sobon, G.; Tarka, J.; Jagiello, J.; Macherzynski, W.; Lipinska, L.; Abramski, K.M. Mode-locked Er-doped fiber laser based on liquid phase exfoliated Sb₂Te₃ topological insulator. *Laser. Phys.* **2014**, *24*, 105111. [[CrossRef](#)]
57. Sotor, J.; Sobon, G.; Macherzynski, W.; Paletko, P.; Abramski, K.M. Black phosphorus saturable absorber for ultrashort pulse generation. *Appl. Phys. Lett.* **2015**, *107*, 051108. [[CrossRef](#)]
58. Luo, Z.C.; Liu, M.; Guo, Z.N.; Jiang, X.F.; Luo, A.P.; Zhao, C.J.; Yu, X.F.; Xu, W.C.; Zhang, H. Microfiber-based few-layer black phosphorus saturable absorber for ultra-fast fiber laser. *Opt. Express* **2015**, *23*, 20030–20039. [[CrossRef](#)]
59. Chen, H.; Li, L.; Ruan, S.C.; Guo, T.; Yan, P.G. Fiber-integrated tungsten disulfide saturable absorber (mirror) for pulsed fiber lasers. *Opt. Eng.* **2016**, *55*, 081318. [[CrossRef](#)]
60. Jiang, Z.K.; Chen, H.; Li, J.R.; Yin, J.D.; Wang, J.Z.; Yan, P.G. 256 fs, 2 nJ soliton pulse generation from MoS₂ mode-locked fiber laser. *Appl. Phys. Express* **2017**, *10*, 122702. [[CrossRef](#)]
61. Mao, D.; She, X.Y.; Du, B.B.; Yang, D.X.; Zhang, W.D.; Song, K.; Cui, X.Q.; Jiang, B.Q.; Peng, T.; Zhao, J.L. Erbium-doped fiber laser passively mode locked with few-layer WSe₂/MoSe₂ nanosheets. *Sci. Rep.* **2016**, *6*, 23583. [[CrossRef](#)] [[PubMed](#)]

62. Zhang, R.L.; Wang, J.; Zhang, X.Y.; Lin, J.T.; Li, X.; Kuan, P.W.; Zhou, Y.; Liao, M.S.; Gao, W.Q. Mode-locked fiber laser with MoSe₂ saturable absorber based on evanescent field. *Chin. Phys. B* **2019**, *28*, 014207. [[CrossRef](#)]
63. Feng, J.J.; Li, X.H.; Feng, T.C.; Wang, Y.M.; Liu, J.; Zhang, H. Harmonic mode-locked Er-doped fiber laser by evanescent field-based MXene Ti₃C₂T_x (T= F, O, or OH) saturable absorber. *Ann. Phys.* **2020**, *532*, 1900437. [[CrossRef](#)]
64. Lu, L.; Liang, Z.M.; Wu, L.M.; Chen, Y.X.; Song, Y.F.; Dhanabalan, S.C.; Ponraj, J.S.; Dong, B.Q.; Xiang, Y.J.; Xing, F.; et al. Few-layer bismuthene: Sonochemical exfoliation, nonlinear optics and applications for ultrafast photonics with enhanced stability. *Laser. Photonics Rev.* **2018**, *12*, 1700221. [[CrossRef](#)]
65. Zhao, Z.H.; Jin, L.; Set, S.Y.; Yamashita, S.J. 2.5 GHz harmonic mode locking from a femtosecond Yb-doped fiber laser with high fundamental repetition rate. *Opt. Lett.* **2021**, *46*, 3621–3624. [[CrossRef](#)]
66. Grelu, P.; Soto-Crespo, J.M. Multisoliton states and pulse fragmentation in a passively mode-locked fibre laser. *J. Opt. B Quantum Semiclass. Opt.* **2004**, *6*, S271. [[CrossRef](#)]
67. Sulimany, K.; Lib, O.; Masri, G.; Klein, A.; Fridman, M.; Grelu, P.; Gat, O.; Steinberg, H. Bidirectional soliton rain dynamics induced by casimir-like interactions in a graphene mode-locked fiber laser. *Phys. Rev. Lett.* **2018**, *121*, 133902. [[CrossRef](#)]
68. Grudinin, A.B.; Gray, S. Passive harmonic mode locking in soliton fiber lasers. *JOSA B* **1997**, *14*, 144–154. [[CrossRef](#)]
69. Loh, W.H.; Grudinin, A.B.; Afanasjev, V.V.; Payne, D.N. Soliton interaction in the presence of a weak nonsoliton component. *Opt. Lett.* **1994**, *19*, 698–700. [[CrossRef](#)]
70. Kutz, J.N.; Collings, B.C.; Bergman, K.; Knox, W.H. Stabilized pulse spacing in soliton lasers due to gain depletion and recovery. *IEEE J. Quantum Electron.* **1998**, *34*, 1749–1757. [[CrossRef](#)]

Disclaimer/Publisher's Note: The statements, opinions and data contained in all publications are solely those of the individual author(s) and contributor(s) and not of MDPI and/or the editor(s). MDPI and/or the editor(s) disclaim responsibility for any injury to people or property resulting from any ideas, methods, instructions or products referred to in the content.